Cross section for aluminum K-shell ionization by oxygen ions*

Roman Laubert and William Losonsky
Department of Physics, New York University, New York, New York 10003
(Received 19 July 1976)

Experimental Al(K) x-ray production cross sections are reported for atomic oxygen projectiles incident on solid aluminum targets with kinetic energy E in the range $0.15 \leq E \leq 91$ MeV from which Al K-shell ionization cross sections are deduced for the projectile energy range $1 \leq E \leq 91$ MeV. For $E \lesssim 1$ MeV nearly all observed x rays are caused by the recoiling aluminum atoms. The results are compared with theories of Coulomb ionization to the target continuum. Differences between experiment and these theories are examined with respect to contributions to inner-shell ionization from electon capture and Pauli excitation. It is found that Coulomb ionization is the dominant process for projectile velocities $v_1 > 4$ a.u., while Pauli excitation dominates when $v_1 < 4$ a.u. Electron-capture processes are significant at high energies, but are negligible for $v_1 < 4$ a.u. for this projectile target system.

I. INTRODUCTION

In the past few years much progress has been made in the study of inner-shell vacancy production in swift heavy-ion-atom collisions, and of various phenomena relating to accurate experimental determinations of these cross sections.[1] New noncharacteristic radiation (NCR) consisting of x-ray bands has been discovered[2]; the importance of recoils in producing x rays has been indicated[3,4]; possible large changes in fluorescence yield are receiving attention[5,6]; the importance of multiple vacancy states in the x-ray emission spectrum has been established[7-9]; and variations in x-ray production cross sections with projectile charge state have been observed experimentally.[10]

To explore the influence of these phenomena in one system, we measured x-ray production cross sections over a very large projectile energy range. We chose oxygen bombardment of solid aluminum targets in the range 0.1–91 MeV. This choice of target-projectile combination is at an intermediate value of the ratio of the projectile atomic number Z_1 to the target-atom atomic number Z_2 ($Z_1/Z_2 = 0.62$), and thus may span the range from Coulomb ionization at high projectile velocities to Pauli excitation at low velocities. This might lead to increased understanding of the various competing mechanisms for producing inner-shell vacancies: Coulomb ionization to the target continuum (the plane-wave Born and the perturbed-stationary-state approximations), electron capture, and Pauli excitation.

Section II describes the experiment and the method of data analysis. Section III reports the measurement of the x-ray production cross sections in an atomic oxygen projectile–aluminum target atom collision. Section II deduces the Al (K)-hole production cross sections in these collisions, and compares experimental results to various theories. We present a summary of our conclusions in Sec. V.

II. EXPERIMENTAL

In this section, we describe the experimental arrangement and method of data analysis up to the point where the experimental cross section for Al (K) x-ray production Σ_x is determined. The experiments were performed with O ions except that a limited number of similar measurements with O_2 ions were made at 1–3 MeV per incident atom. We first consider the thick-target measurements, then those for thin targets.

A. Thick-target measurements

The New York University heavy-ion accelerator provided O^+ projectiles in the energy range 0.10–0.32 MeV, and the Brookhaven National Laboratory 3-MeV Van de Graaff accelerator was the source of O^+ projectiles in the energy range 0.37–3 MeV. The apparatus is similar to that described[11] earlier. A monoenergetic $^{16}O^+$ ion beam strikes a thick target (~0.1 mm) of high-purity aluminum. The target is set at 45° with respect to the ion beam axis and to the line of sight of the x-ray detector. The x-rays are detected by a Si(Li) detector and the spectrum is stored in a multichannel analyzer. We performed the experiment over the entire energy range with two Si(Li) detectors having different beryllium window thicknesses, 25- and 8-μm, and energy resolutions, respectively, of ~250 and 190 eV full width at half maximum. Sample spectra from the detector with the 8-μm window appear in Fig. 1, along with the detector efficiency ϵ (in the inset). The detector efficiency was calculated using the manufacturer's specifications to include the effects of x-ray attenuation by the beryllium window, gold electrode layer, and silicon dead layer. The gold and silicon absorp-

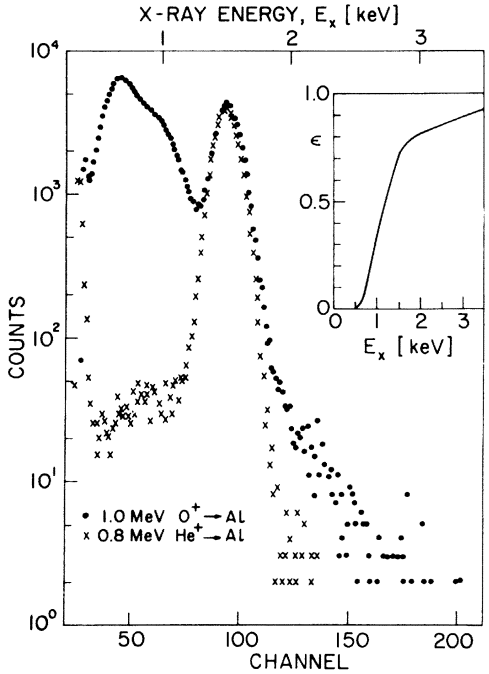

FIG. 1. Typical x-ray spectra for ions incident on a thick solid-aluminum target using a Si(Li) detector with an 8-μm beryllium window. The inset shows the detector efficiency. (Absorption edges of gold and silicon are not shown in this figure.)

tion edges have been neglected because they change ϵ by only ±4%, which is less than the accuracy of the detector efficiency. The detector efficiency for Al(K) x rays, ϵ_{Al}, was calculated to be 0.39 and 0.70 for the detectors with 25- and 8-μm windows respectively. The x-ray spectrum from O^+ bombardment (shown in Fig. 1 as circles) consists of the Al(K) peak at 1.5 keV and a broad band extending from our lowest detectable energy (~0.7 keV for the 8-μm window) to ~2.7 keV. This is the NCR band, which is attributed to the deexcitation of holes in quasimolecular levels during collisions.[2] The extent of this band may be seen by comparing in Fig. 1 the x-ray spectrum for incident oxygen projectiles with that for incident helium ions. For our purposes the NCR band represents a background which must be subtracted from the spectrum so that we can integrate the counts in the Al(K) peak to determine the measured Al(K) x-ray yield $Y_x(E)$ at projectile energy E.

We extract $Y_x(E)$ from the spectrum by computer fitting procedures. Since the shape of the observed band depends markedly on the detector window, different procedures were used for the data taken with the different detector windows. For the data taken with the 25-μm window detector the background noise was subtracted and the spectrum fitted to two Gaussians whose six parameters were determined by a search routine which minimized χ^2. Both the NCR band and the Al(K) peak were found to be Gaussian to better than two standard deviations on each side of the maximum. For data taken with the 8-μm window detector, the contribution of the band could be determined by using a small segment of the band spectrum on each side of the Al(K) peak to interpolate the band spectrum under it.

The yield $Y_x(E)$ was measured for a pre-set number of incident projectiles N by integrating the beam current at the biased target. The Al(K) x-ray yield per incident particle is

$$Y(E)=\frac{Y_x(E)}{N}\frac{4\pi}{\Omega_x}\frac{1}{\epsilon_{Al}}, \tag{1}$$

where Ω_x is the solid angle of the x-ray detector seen from the target.

The $Y(E)$ values found by averaging the results obtained for the 8- and 25-μm window data (a total of ~140 runs) are shown in Fig. 2 as circles and listed in column 2 of Table I. Also shown in Fig. 2, as triangles, are yields per incident projectile of x rays in the NCR band for the case of the 8-μm window detector. The NCR band yields per incident projectile for the 25-μm window data show the same trends, but are smaller by a factor of ~10. In Fig. 3 we show the ratio R of the characteristic

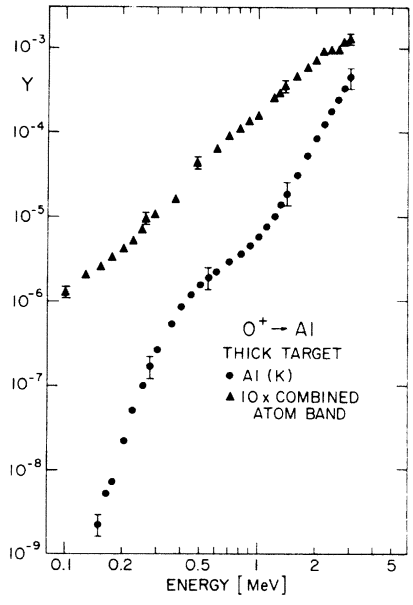

FIG. 2. Total x-ray yields per incident atom from O^+ bombardment of a thick solid-aluminum target as a function of projectile energy: (●) Al(K) yield, corrected for window absorption and detector geometry, (▲) ten times the observed NCR band yield for the 8-μm beryllium window detector, corrected for geometry only.

TABLE I. Aluminum K-shell x-ray production cross sections $\sigma_x(E)$ for incident $^{16}O^+$ particles of energy E. Column 2 is the thick-target Al(K) x-ray yield $Y(E)$, in x rays per incident particle. Column 3 is the derivative of $Y(E)$ with respect to E. Column 4 is the total stopping power $S(E)/\rho$, in keV cm$^2/\mu$g, for ^{16}O particles in aluminum, where ρ is the mass density of aluminum. Column 5, labeled $\sigma_{corr}(E)$, is the sum of two correction terms to $\Sigma_x(E)$: the absorption correction $[\mu Y(E)/N_2]$, and the straggling correction $-\int d\sigma(E,T)[Y(E-T)-Y(E)+TdY(E)/dE]$, in barns. Column 6 is the total Al(K) x-ray production cross section $\Sigma_x(E)$ in barns, as determined by Eq. (2), i.e. $\Sigma_x(E)=[S(E)Y'(E)]/N_2+\sigma_{corr}(E)$. Column 7 is the recoil contribution $\sigma_{xR}(E)$, in barns, as determined by Eq. (5) and explained in the text. Column 8 gives the values for $\sigma_x(E)$ in barns as determined by Eq. (4). For these computations μ/ρ is 396 cm^2/g and N_2/ρ is 2.23×10^{16} atoms/μg. Numbers in parentheses are powers of ten. Error bars quoted are 1 SD in the absolute error.

Energy E (MeV)	$Y(E)$ (x rays/particle) ±30%	$dY(E)/dE$ (x rays/keV particle) ±30%	$S(E)$ (keV cm$^2/\mu$g) ±15%	$\sigma_{corr}(E)$ (b)	$\Sigma_x(E)$ (b) ±30%	$\sigma_{xR}(E)$ (b)	$\sigma_x(E)$ (b)
0.150	2.22(−9)	1.28(−10)	1.78	−4.6(−4)	9.21(−3)	1.85(−2)	•••
0.165	5.14(−9)	2.61(−10)	1.85	−7.2(−4)	2.08(−2)	3.61(−2)	•••
0.175	7.12(−9)	3.71(−10)	1.88	−9.3(−4)	3.10(−2)	5.23(−2)	•••
0.200	2.24(−8)	8.09(−10)	1.97	−1.6(−3)	7.08(−2)	1.08(−1)	•••
0.225	5.08(−8)	1.46(−9)	2.07	−2.7(−3)	1.35(−1)	1.83(−1)	•••
0.250	9.78(−8)	2.33(−9)	2.16	−3.1(−3)	2.26(−1)	2.73(−1)	•••
0.275	1.70(−7)	3.34(−9)	2.26	−3.0(−3)	3.37(−1)	3.72(−1)	•••
0.300	2.65(−7)	4.36(−9)	2.36	−2.3(−3)	4.60(−1)	4.76(−1)	•••
0.350	5.28(−7)	6.00(−9)	2.53	+2.6(−3)	6.82(−1)	6.82(−1)	•••
0.400	8.48(−7)	6.88(−9)	2.72	1.2(−2)	8.48(−1)	8.68(−1)	•••
0.450	1.19(−6)	7.16(−9)	2.90	1.9(−2)	9.47(−1)	1.03(0)	•••
0.500	1.56(−6)	7.00(−9)	3.08	2.5(−2)	9.97(−1)	1.17(0)	•••
0.550	1.91(−6)	6.68(−9)	3.26	3.2(−2)	1.03(0)	1.30(0)	•••
0.600	2.23(−6)	6.44(−9)	3.44	3.7(−2)	1.05(0)	1.41(0)	•••
0.700	2.89(−6)	6.76(−9)	3.76	4.9(−2)	1.22(0)	1.59(0)	•••
0.800	3.65(−6)	8.23(−9)	4.02	6.2(−2)	1.56(0)	1.71(0)	•••
0.900	4.60(−6)	1.11(−8)	4.24	7.9(−2)	2.19(0)	1.79(0)	•••
1.00	5.91(−6)	1.54(−8)	4.44	1.0(−1)	3.22(0)	1.83(0)	1.39(0) ±80%
1.10	7.76(−6)	2.17(−8)	4.63	1.3(−1)	4.66(0)	1.86(0)	2.80(0) ±55%
1.20	1.03(−5)	2.99(−8)	4.80	1.7(−1)	6.65(0)	1.86(0)	4.79(0) ±45%
1.30	1.39(−5)	4.03(−8)	4.93	2.4(−1)	9.42(0)	1.85(0)	7.57(0) ±40%
1.40	1.90(−5)	5.31(−8)	5.04	3.2(−1)	1.25(+1)	1.83(0)	1.07(+1) ±35%
1.60	3.12(−5)	8.40(−8)	5.32	5.3(−1)	2.06(+1)	1.78(0)	1.88(+1) ±30%
1.80	5.21(−5)	1.26(−7)	5.56	8.9(−1)	3.25(+1)	1.72(0)	3.08(+1) ±30%
2.00	8.22(−5)	1.75(−7)	5.76	1.4(0)	4.65(+1)	1.66(0)	4.48(+1) ±30%
2.20	1.22(−4)	2.24(−7)	5.95	2.1(0)	6.18(+1)	1.59(0)	6.02(+1) ±30%
2.40	1.72(−4)	2.98(−7)	6.11	3.0(0)	8.45(+1)	1.53(0)	8.30(+1) ±30%
2.60	2.39(−4)	3.83(−7)	6.26	4.2(0)	1.12(+2)	1.47(0)	1.11(+2) ±30%
2.80	3.26(−4)	4.84(−7)	6.37	5.7(0)	1.44(+2)	1.41(0)	1.43(+2) ±30%
3.00	4.34(−4)	6.04(−7)	6.50	7.6(0)	1.84(+2)	1.36(0)	1.83(+2) ±30%

Al(K) x-ray yield to the NCR band yield as a function of the incident ion energy as recorded using the 8-μm window detector. The NCR band yield in Fig. 2 and the yields in Fig. 3 are not corrected for detector efficiency. The characteristic Al(K) x rays dominate at large incident ion energies while the noncharacteristic x rays are dominant at low incident ion energies. Below 0.15-MeV ion energy the yield of Al(K) x rays is so small that we could not resolve values for this ratio.

The total cross section for Al(K) x-ray production $\Sigma_x(E)$ can be determined from the formula,[3,4,12] valid for our geometry

$$\Sigma_x(E)=\frac{1}{N_2}\left[\frac{dY(E)}{dE}S(E)+\mu Y(E)\right] - \int d\sigma(E,T)\left[Y(E-T)+T\frac{dY(E)}{dE}-Y(E)\right]. \quad (2)$$

Here N_2 is the atomic density of the aluminum target, $S(E)$ the total stopping power of the target for oxygen atoms of energy E, μ the absorption coefficient of the target for its own characteristic x ray, and $d\sigma(E,T)$ the differential cross section for transfer of energy T from the projectile to the tar-

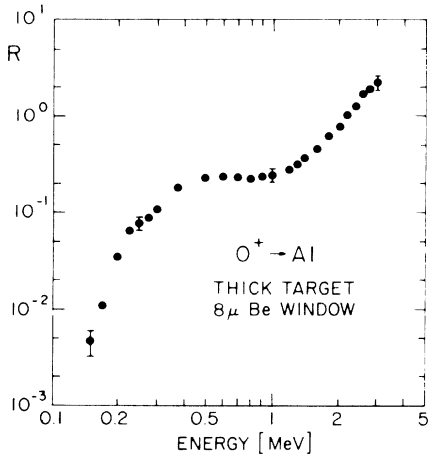

FIG. 3. Ratio R of measured Al(K) x-ray yield to the measured NCR band yield for O^{+} bombardment of a thick aluminum target obtained with the 8-μm beryllium window detector. No corrections are made for detector efficiency.

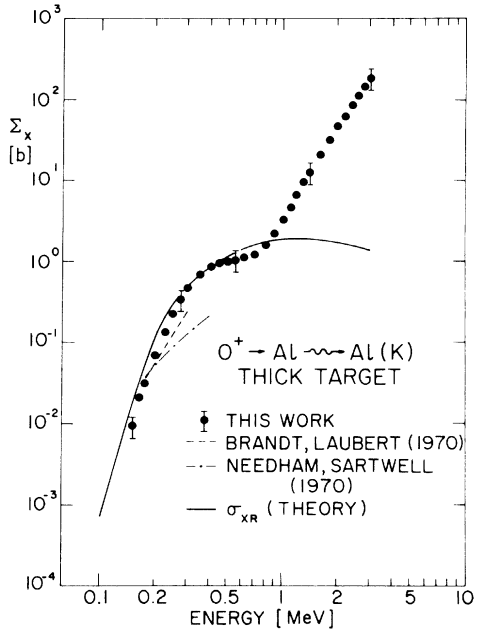

FIG. 4. Cross sections for Al(K) x-ray production in barns for O^{+} bombardment of a thick solid-aluminum target as a function of projectile energy in MeV: (●) our experimental $\Sigma_x(E)$ values determined using Eq. (2), (--- and — • —) other experimental values taken from Refs. 18 and 17 respectively. The solid curve is the recoil contribution $\sigma_{xR}(E)$ calculated using Eq. (5) as described in the text.

get atom in a collision. We determine $S(E)$, column 4 of Table I, by adding to the electronic stopping power[13-15] the theoretical nuclear stopping power.[16] For $d\sigma(E,T)$ we used the theoretical values obtained for scattering of a charged particle in a Coulomb field screened by a Thomas-Fermi potential.[16] If the integrand in Eq. (2) is neglected, one recovers the standard formula,[12] of which the term $\mu Y(E)/N_2$ is a correction for absorption of x rays in the target, at most 5% in our experiment. The integrand, obtained by Taulbjerg *et al.*,[3,4] may be interpreted as a correction due to energy straggling of the projectile. In our case this term is also always $\leq 5\%$ of Σ_x.

Equation (2) was used to extract values of $\Sigma_x(E)$ separately for the data taken with the 8- and 25-μm window detectors. The results were averaged to obtain the Σ_x values shown in Fig. 4 as circles, and listed in column 6 of Table I. The values of $Y(E)$ shown in Fig. 2 result in Σ_x values which are well within the quoted error bars. Included in the figure are previous thick-target results taken with proportional counters. The results of Needham and Sartwell[17] do not seem to subtract the NCR band, while the results of Brandt and Laubert[18] only partially take it into account by using x-ray absorbers, causing differences in the slopes of the data.

The Al(K) x-ray distribution after subtraction of the NCR band yields the centroid of the Al(K) line. From it the shift in energy of the observed Al(K) x-ray line can be determined relative to the expected peak position if only a K vacancy existed in the aluminum atom. In Fig. 5, $\Delta E_K(E)$, the resulting energy shift, is shown as a function of beam energy. An average of all runs (from 4–16) at each energy is shown. The error bar is ±12 eV, due about equally to uncertainty in the channel position of the observed Al(K) peak, fixing the position of the unshifted Al(K) peak, and energy calibration. See Sec. IV for further discussion of this curve.

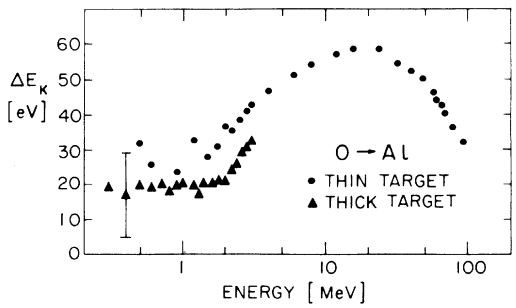

FIG. 5. Measured Al(K) x-ray centroid shift ΔE_K in eV, from the x-ray energy when only a K hole is produced in aluminum, as a function of projectile energy in MeV for oxygen-ion bombarding: (●) thin solid targets, (▲) thick solid targets.

B. Thin target measurements

Measurements were performed at the Brookhaven National Laboratory with the 3-MeV Van de Graaff accelerator in the energy range of 0.53–3 MeV, and with the Tandem Van de Graaff accelerator in the energy range 2–91 MeV.

The apparatus used in the tandem experiment is the same as that described[19,20] earlier. A monoenergetic $^{16}O^+$ beam is incident on a thin (~20 $\mu g/cm^2$) self-supporting aluminum target[21] inclined 45° with respect to the beam direction. At beam energies $E > 3$ MeV, higher charge states of oxygen were used (up to +8 at 91 MeV), but the resulting x-ray cross sections at the high energies are known[19] to be independent of the incident atom's charge state for targets of the thickness employed here. For completeness, the incident projectile charge state for the tandem experiment is listed in column 2 of Table III. A Si(Li) x-ray detector views the beam exit surface of the target at 45° to the target surface normal and 90° to the beam direction. Data were taken with both the 8- and 25-μm window detectors with the 3-MeV machine. For the tandem experiment, where the yields from the NCR band are relatively small, data were taken only with the 25-μm window detector. The target was also viewed at a variable angle with respect to the beam direction by a silicon surface-barrier detector, which registered the energy distribution of particles scattered in the oxygen-aluminum collisions. The angle was fixed at 45° for projectile energies ≤ 3 MeV, but at higher energies was shifted to smaller angles (as small as 8° at 91 MeV). At energies greater than 3-MeV data were taken at several angles. Such precautions were necessary to insure that the experiments were performed under conditions where the effects of the finite nuclear sizes of the colliding atoms is negligible and the Rutherford scattering law is obeyed. For example, at a projectile energy of 91 MeV and a laboratory scattering angle as small as 20°, the error introduced by assuming Rutherford scattering would be several times larger than the uncertainties quoted in Table III.[22] The outputs of the x-ray and particle detectors were amplified and stored separately in a pulse-height analyzer.

The Al(K) x-ray production cross section in the thin-target approximation is

$$\Sigma_x(E) = \frac{Y_x(E)}{N_s(E)} \frac{\Omega_D}{\Omega_x} \frac{4\pi}{\epsilon_{Al}} \left(\frac{d\sigma(E)}{d\Omega}\right)_R , \tag{3}$$

where $Y_x(E)$ is the measured Al(K) x-ray yield at projectile energy E, $N_s(E)$ the number of elastically scattered oxygen projectiles recorded at the same time as $Y_x(E)$, Ω_D, and Ω_x are the solid angles subtended at the target by the particle and x-ray detectors respectively, and $[d\sigma(E)/d\Omega]_R$ denotes the differential Rutherford scattering cross section. We extract $Y_x(E)$ from the x-ray spectrum in the same manner as for thick targets. The data taken on the tandem were analyzed by use of the program "Brutal".[20] This program gave the same results for thin-target data taken at $E \geq 2$ MeV as the method used for thick targets. The average energy shift of the Al(K) x ray, $\Delta E_K(E)$, for thin targets is shown in Fig. 5. Average values of $\Sigma_x(E)$, for two to nine determinations at each energy, are listed in column 2 of Table II and in column 3 of Table III.

Measurements were also made with molecular oxygen (O_2^+ and O_2^-) beams at energies of 1–3 MeV per incident atom. If one compares the measured x-ray yield per incident atom at the same velocity, the yields are found, for both the NCR band and the Al(K) peak, to be independent (to ±5%) of whether O_2^+, O_2^-, or O^+ projectiles are employed.

III. ANALYSIS OF TOTAL X-RAY PRODUCTION CROSS SECTIONS

A. Thick target

We make use of recent advances[3,4] in analyzing thick-target data by applying the equation

$$\Sigma_x(E) = \sigma_x(E) + \sigma_{xR}(E) , \tag{4}$$

where $\sigma_x(E)$ is the cross section for Al(K) x-ray production in the collision of an oxygen atom with an aluminum atom, averaged over the equilibrium charge and excitation states of the projectile of energy E in the solid. It is the quantity of interest. The cross section for producing an Al(K) x ray by a recoiling aluminum atom striking other target atoms, $\sigma_{xR}(E)$, is given by[4]

$$\sigma_{xR}(E) = \int d\sigma(E,T) f(T,E,\theta) Y_R(T,\theta) , \tag{5}$$

where $Y_R(T,\theta)$ is the thick-target Al(K) x-ray yield for aluminum projectiles of energy T striking a solid aluminum target where θ is the angle between the surface normal and the beam direction, and $f(T,E,\theta)$ is an angular-dependent factor given in Ref. 4. Under our conditions the effect of $f(T,E,\theta)$ is small. Hence we have suppressed the θ dependence in writing $\sigma_{xR}(E)$.

We have calculated $\sigma_{xR}(E)$ from Eq. (5) by a numerical integration procedure with $d\sigma(E,T)$ as in Sec. II A. For $Y_R(T,\theta)$ we employed experimental values[4,23] in the energy range 0.08–40 MeV and extrapolation procedures for energies <0.08 MeV. A variety of extrapolation procedures were tried and convinced us that to ±10% the form of the extrapolation was not crucial in determining $\sigma_{xR}(E)$ in our energy range. The function $f(T,E,\theta)$ was included in our computations of $\sigma_{xR}(E)$, but re-

TABLE II. Aluminum K-shell x-ray production cross sections $\sigma_x(E)$, for incident $^{16}O^+$ particles of energy E. These measurements are for thin targets, taken on the 3-MeV Brookhaven National Laboratory Van de Graaff. Column 2 is the total thin-target Al(K) x-ray production cross section in the thin-target approximation [Eq. (3) in the text]. Column 3 gives α_s, the correction factor to the number of scattered particles. Column 4 gives α_x, the correction factor to the x-ray yield. Column 5 gives the yield correction due to angular scattering of incident particles in the foil. Column 6 is the yield correction term for recoils. Column 7 gives the values of $\sigma_x(E)$ in barns as determined from $\Sigma_x(E)$ in column 2 by Eq. (7), utilizing the corrections in columns 3–6. Numbers in parentheses indicate powers of 10. Error bars quoted are 1 SD in absolute error.

Energy E (MeV)	$\Sigma_x(E)$ (b) ±20%	$\alpha_s(E)$	$\alpha_x(E)$	$Y_s(E)/Y_E(E)$	$Y_R(E)/Y_E(E)$	$\sigma_x(E)$ (b) ±25%
1.00	1.72(+0)	1.14	0.746	−1.3(−2)	3.8(−1)	...
1.20	4.24(+0)	1.12	0.771	−8.7(−3)	1.4(−1)	5.69(+0)
1.40	9.15(+0)	1.11	0.787	−6.8(−3)	6.4(−2)	1.19(+1)
1.60	1.68(+1)	1.10	0.800	−5.5(−3)	3.3(−2)	2.24(+1)
1.80	3.04(+1)	1.09	0.811	−4.4(−3)	1.8(−2)	3.92(+1)
2.00	5.24(+1)	1.09	0.822	−3.6(−3)	1.0(−2)	6.48(+1)
2.20	7.21(+1)	1.08	0.831	−2.9(−3)	6.2(−3)	1.02(+2)
2.40	1.18(+2)	1.08	0.839	−2.3(−3)	4.1(−3)	1.54(+2)
2.60	1.71(+2)	1.07	0.846	−1.8(−3)	2.6(−3)	2.26(+2)
2.80	2.47(+2)	1.07	0.853	−1.5(−3)	1.8(−3)	3.22(+2)
3.00	3.32(+2)	1.06	0.856	−1.2(−3)	1.3(−3)	4.47(+2)

placing this factor by unity results in a negligible change in $\sigma_{xR}(E)$ at low energies, a 15% increase at 1 MeV, and about a 25% increase at 3 MeV. In Fig. 4 we plot (solid line) the function $\sigma_{xR}(E)$ and list its value in column 7 of Table I.

An analytic calculation of $\sigma_{xR}(E)$ with

$$Y_R(E,\theta) = [C(E/B)^{1/2} + (B/E)^{1/2} - 2] \quad \text{for } E \geq B$$
$$= 0 \quad \text{for } E < B \qquad (6)$$

where $C = 5.41 \times 10^{-3}$ x rays per incident aluminum atom and $B = 142$ keV, Rutherford scattering for

TABLE III. Aluminum K-shell x-ray production cross sections $\sigma_x(E)$, for incident $^{16}O^{+q}$ particles of energy E. These measurements are for thin targets, taken on the Brookhaven National Laboratory Tandem Van de Graaff. Column 2 is the charge state of the incident projectile. Columns 3–8 follow 2–7 of Table II. Numbers in parentheses indicate powers of 10. Error bars quoted are 1 SD in absolute error.

Energy E (MeV)	q	$\Sigma_x(E)$ (b) ±20%	$\alpha_s(E)$	$\alpha_x(E)$	$Y_s(E)/Y_E(E)$	$Y_R(E)/Y_E(E)$	$\sigma_x(E)$ (b)
2.00	1	4.38(+1)	1.09	0.815	−2.9(−3)	1.2(−1)	5.73(+1) ±25%
3.00	1	2.64(+2)	1.06	0.867	−1.0(−3)	1.6(−3)	3.24(+2) ±25%
4.00	2	9.33(+2)	1.05	0.891	−5.3(−4)	4.0(−4)	1.10(+3) ±25%
6.00	2	3.89(+3)	1.04	0.937	−1.6(−4)	8.1(−5)	4.30(+3) ±20%
8.00	2	9.16(+3)	1.03	0.954	−4.9(−5)	3.0(−5)	9.86(+3) ±20%
12.0	3	2.76(+4)	1.02	0.970	−3.8(−5)	7.8(−6)	2.89(+4) ±20%
16.0	3	4.19(+4)	1.01	0.978	−9.7(−6)	4.2(−6)	4.33(+4) ±20%
24.0	4	8.33(+4)	1.01	0.985	−1.6(−6)	1.8(−6)	8.51(+4) ±20%
32.0	4	9.62(+4)	1.00	0.988	−2.8(−6)	1.4(−6)	9.78(+4) ±20%
40.0	5	1.03(+5)	1.00	0.989	−1.3(−6)	1.2(−6)	1.05(+5) ±20%
48.0	6	1.05(+5)	1.00	0.989	−2.9(−6)	1.1(−6)	1.06(+5) ±20%
57.0	6	8.22(+4)	1.00	0.989	−4.5(−6)	1.2(−6)	8.33(+4) ±20%
60.0	6	9.42(+4)	1.00	0.989	−1.1(−6)	1.1(−6)	9.54(+4) ±20%
67.0	6,7	7.15(+4)	1.00	0.990	−4.2(−6)	1.3(−6)	7.24(+4) ±20%
78.0	8	6.57(+4)	1.00	0.990	−2.7(−6)	1.4(−6)	6.65(+4) ±20%
91.0	8	6.05(+4)	1.00	0.990	−1.4(−6)	1.4(−6)	6.12(+4) ±20%

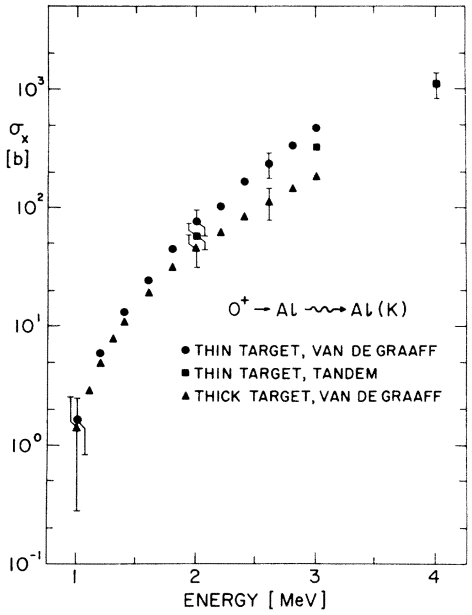

FIG. 6. Our experimentally determined Al(K) x-ray production cross sections, $\sigma_x(E)$, in barns, for O^+ bombardment of solid aluminum targets as a function of projectile energy in MeV, for $E \leq 4$ MeV: (●) thin-target values using the Van de Graaff accelerator, (■) thin-target values using the tandem Van de Graaff accelerator, (▲) thick-target values.

$d\sigma(E,T)$, and $f(T,E,\theta)=1$ [this is equivalent to Eq. (13) in Ref. 24] produces $\sigma_{xR}(E)$ values with the same trends as the curve in Fig. 4, but distinct differences appear at low and high energies.

From this analysis we conclude that at $E \leq 1$ MeV nearly all of the observed x rays are due to target-atom recoils, while at higher energies nearly all x rays are due to projectile target-atom collisions. We subtract $\sigma_{xR}(E)$ from $\Sigma_x(E)$ to extract $\sigma_x(E)$ values from our thick-target measurements for $E \geq 1$ MeV. These values are shown as triangles in Fig. 6 and listed in column 8 of Table I.

B. Thin target

For values of $\Sigma_x(E)$ for thin targets given by Eq. (3) we obtain cross sections $\sigma_x(E)$ for Al(K) x-ray production in the collision of an oxygen atom with an aluminum target atom from the equation

$$\sigma_x(E)=\Sigma_x(E)\,\frac{\alpha_s(E)}{\alpha_x(E)}\left(1-\frac{Y_s(E)+Y_R(E)}{Y_E(E)}\right), \qquad (7)$$

which is developed in Ref. 20. Here $\alpha_s(E)$ is a correction factor[23] to the number of scattered particles $N_s(E)$, arising from energy loss in the finite thickness aluminum foil; $\alpha_x(E)$ is a correction factor[23] to the x-ray yield $Y_x(E)$, arising from x-ray absorption and projectile energy loss in the foil; $Y_s(E)$ is a yield correction due to angular scattering of incident particles in the foil; $Y_R(E)$ is the x-ray yield contribution due to recoil target atoms colliding with other target atoms; and $Y_E(E)$ is $\Sigma_x(E)N_2\alpha_s(E)$. The recoil yield Y_R behaves similarly to the contribution for thick targets in that it is negligible at high energies and dominant for $E<1$ MeV: already at 1 MeV, Y_R is ~40% of Y_E. This precludes obtaining accurate values of σ_x for $E \leq 1$ MeV. Average values of $\alpha_s(E)$, $\alpha_x(E)$, $Y_s(E)/Y_E(E)$, and $Y_R(E)/Y_E(E)$ are given in columns 3–6 of Table II for the Van de Graaff data, and in columns 4–7 of Table III for the Tandem Van de Graaff data. For further details of the methods of calculation consult Ref. 20.

These corrections were performed separately on the data for the 8- and 25-μm window detectors (a total of ~60 runs) and the resulting cross sections averaged to obtain $\sigma_x(E)$ values for the Van de Graaff data, shown as circles in Fig. 6 and listed in column 7 of Table II. Our x-ray cross sections for the tandem data (~40 runs) were averaged to obtain a single value at each energy; they are listed in column 8 of Table III, and shown as squares in Fig. 6 for the region of overlap with our other values. It is important to note that in both Tables II and III average values of all quantities at each energy are given. Thus $\sigma_x(E)$ values in the last column may not be exactly equal to the values obtained by combining the results given in the previous columns, since these calculations are performed separately for each run and then averaged. Nevertheless, if one does compute $\sigma_x(E)$ from the values listed in the tables, resulting values of $\sigma_x(E)$ will be well within the error bars quoted.

The target thicknesses are expected to be sufficient to establish charge equilibrium[19]; we interpret $\sigma_x(E)$ as for the thick-target values. Thus one should get agreement between the thick and thin $\sigma_x(E)$ values. This can be seen in Fig. 6 to be generally the case, although there is a tendency for the thick-target values to be somewhat low at the highest energies.

C. Comparison with other measurements

We determine best values of $\sigma_x(E)$ from the values for thick targets (Table I) and those for thin targets (Tables II and III) by an averaging procedure which takes account of the uncertainties in the measurements. These values are listed in column 2 of Table IV and shown as circles in Fig. 7.

By way of comparison we include in Fig. 7 the experimental results of Sakisaka,[25] and of Burch and Richard.[26] Sakisaka's data are a factor of 5 larger than ours near $E=1$ MeV. However, his results predate the discovery of the NCR band and

TABLE IV. Aluminum K-hole production cross sections $\sigma_K(E)$, for ^{16}O ions of energy E incident on solid aluminum targets. Column 2 is the x-ray production cross section $\sigma_x(E)$, from both thick- and thin-target measurements. Column 3 is $\sigma_K(E)$ found from $\sigma_K(E) = \gamma_K^{-1}\sigma_x(E)$, where γ_K is $0.0426 \pm 10\%$. For further discussion of γ_K see the text. Numbers in parentheses indicate powers of 10. Error bars quoted are 1 SD in the absolute errors.

Energy E (MeV)	$\sigma_x(E)$ (b)	$\sigma_K(E)$ (b)
1.00	1.54 ±50%	3.62(+1) ±50%
1.20	5.55 ±30%	1.30(+2) ±30%
1.40	1.20(+1) ±25%	2.82(+2) ±25%
1.60	2.12(+1) ±25%	4.98(+2) ±25%
1.80	3.63(+1) ±25%	8.52(+2) ±25%
2.00	5.59(+1) ±25%	1.31(+3) ±25%
2.20	7.69(+1) ±25%	1.80(+3) ±25%
2.40	1.11(+2) ±25%	2.60(+3) ±25%
2.60	1.52(+2) ±25%	3.57(+3) ±25%
2.80	2.78(+2) ±25%	6.52(+3) ±25%
3.00	3.69(+2) ±25%	8.66(+3) ±25%
4.00	1.10(+3) ±25%	2.60(+4) ±25%
6.00	4.30(+3) ±20%	1.01(+5) ±20%
8.00	9.86(+3) ±20%	2.31(+5) ±20%
12.0	2.89(+4) ±20%	6.78(+5) ±20%
16.0	4.33(+4) ±20%	1.02(+6) ±20%
24.0	8.51(+4) ±20%	2.00(+6) ±20%
32.0	9.78(+4) ±20%	2.30(+6) ±20%
40.0	1.05(+5) ±20%	2.46(+6) ±20%
48.0	1.06(+5) ±20%	2.49(+6) ±20%
57.0	8.33(+4) ±20%	1.96(+6) ±20%
60.0	9.54(+4) ±20%	2.24(+6) ±20%
67.0	7.24(+4) ±20%	1.70(+6) ±20%
78.0	6.65(+4) ±20%	1.56(+6) ±20%
91.0	6.12(+4) ±20%	1.44(+6) ±20%

the importance of recoils in determining cross sections. The high-energy data of Burch and Richard agree better with our data, although differences exceeding the quoted errors exist.

IV. COMPARISON WITH THEORY

High-resolution studies[28-30] of the Al(K) x-ray spectrum for oxygen bombardment of aluminum show satellite peaks, which are attributed to x rays emitted by atoms with n vacancies in the L shell (the KL^n peaks), n ranging from one to six. With our resolution we record a single broad peak shifted in energy $\Delta E_K(E)$ corresponding to the average shift in the KL^n x-ray distribution. Indeed, our $\Delta E_K(E)$ measurements (Fig. 5) agree with values calculated from high-resolution x-ray data[28-30] taken over a limited range of E. Our energy shift measurements indicate a nearly constant value of $\Delta E_K(E)$ for $E < 1$ MeV with an abrupt increase near $E = 1$ MeV. We attribute this change to the decreasing yield of x rays originating from target-recoil collisions. For $E > 1$ MeV, $\Delta E_K(E)$

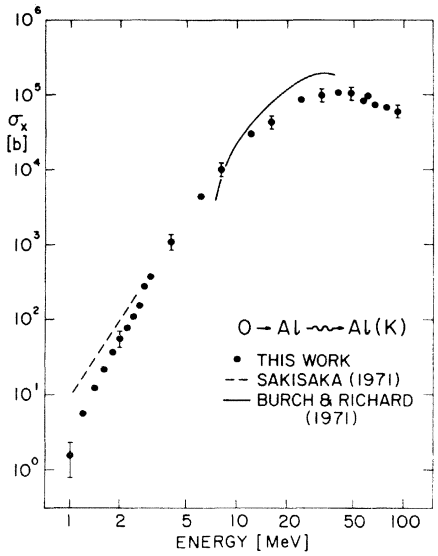

FIG. 7. Experimentally determined Al(K) x-ray production cross sections $\sigma_x(E)$, in barns, for oxygen ions bombarding solid-aluminum targets, as a function of projectile energy in MeV: (•) values for this work, --- Ref. 25, — Ref. 26.

reflects the relative L-shell to K-shell excitation processes in projectile-target atom collisions, with a maximum at $E \sim 20$ MeV. The K x-ray energy shifts by ~12 eV for each L hole present with the K hole at the time of emission.[9,29,30] Figure 5 indicates that there can be on the average as many as four L holes at the time of K x-ray emission.

We must transform our $\sigma_x(E)$ values to total cross sections for Al(K) ionization through the fluorescence yield. The fluorescence yield depends on the number and kind of L holes present in the atom emitting a K x ray. Therefore, we need an average fluorescence yield $\gamma_K(E)$ at each projectile energy.

One determines $\gamma_K(E)$ as follows. From our $\Delta E_K(E)$ measurements and measured values[9,29,30] of the satellite x-ray peak energies we estimate the average number of L holes present during the K x-ray emission. With the theoretical values[29] of the fluorescence yield for the KL^n hole configurations we obtain $\gamma_K(E)/\gamma_0 = 1.12 \pm 4\%$, where γ_0 is the fluorescence yield of aluminum without any L holes present. This value agrees with that determined from measured intensities[29] in the KL^n peaks for oxygen projectile energies of $3 \leq E \leq 30$ MeV. We have assumed in this calculation that all of the L holes are in the $2p$ subshell, which is consistent with measurements on aluminum targets.[9,28-33]

A note of caution. If it turns out that some of the L holes in aluminum producing the observed satellites were to be in $2s$ rather than $2p$ states as

assumed here, then our $\gamma_K(E)$ may be too small by as much as a factor two. Such variation has been calculated for the neon K-shell fluorescence yield where there is a dependence on the multiplet state of the atom.[34]

We consider another method for determining $\gamma_K(E)$. By use of the fractional-parentage coefficient method,[35] and modified Hartree-Fock-Slater calculations of Auger and x-ray transition rates for the KL^0 hole configuration[35] we calculate the K fluorescence yield as a function of the number of L holes in aluminum. Our experimental $\Delta E_K(E)$ results, in conjunction with Hartree-Fock-Slater computations[9] of ΔE_K as a function of the number of L holes, enables us to determine an average number of L holes as a function of projectile energy. Combining these results gives a $\gamma_K(E)/\gamma_0$ which rises from a value of 1.6 at $E = 1.0$ MeV to a maximum value of 2.8 at $E = 20$ MeV and then declines to 1.6 at $E = 91$ MeV. Thus the results of the model based on the fractional-parentage coefficient calculations give values larger than our $\gamma_K(E)$ by approximately a factor three.

Our value of $\gamma_K(E)/\gamma_0 = 1.12$ and the experimentally determined value[36] of 0.038 for γ_0, results in $\gamma_K(E) = 0.0426 \pm 10\%$. We determine $\sigma_K(E)$ from the $\sigma_x(E)$ values in Table IV by using the equation

$$\sigma_K(E) = \sigma_x(E)/\gamma_K(E), \tag{8}$$

where $\sigma_K(E)$ is interpreted as the total cross section for producing K holes in aluminum, averaged over all equilibrium charge and excitation states of the projectile. The values of $\sigma_K(E)$ are listed in column 3 of Table IV and shown as circles in Fig. 8. The dashed line on the error bars in Fig. 8 indicates the shift in σ_K when it is determined using $\gamma_K(E)$ as calculated according to the fractional-parentage coefficient method.

We compare these results to quantum-mechanical cross sections for Coulomb ionization to the target-atom continuum. We also consider other possible competing mechanisms, in particular electron capture and Pauli excitation.

The PWBA prediction[37] is shown in Fig. 8 as the dashed curve. The perturbed-stationary-state (PSS) approximation[38] includes the perturbation of the K shell by the projectile. At low velocities this amounts to an increased binding (B) of the K-shell electrons. On incorporating the Coulomb deflection (C) the theory[39] gives the dot-dash curve in Fig. 8 labeled as PSS(CB). At intermediate velocity the perturbation acts as a polarization (P) of the K shell by the projectile, and the total effect results in the solid line labeled PSS(CBP).[20] It is important to note that although these calculations are based on one-electron transitions they should be compared with the total cross section

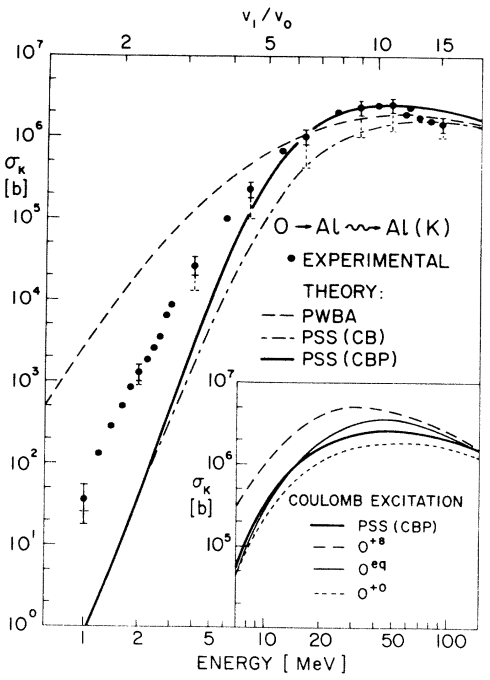

FIG. 8. Ionization cross sections in barns, as a function of projectile energy in MeV (and also as a function of v_1/v_0, where v_1 is the projectile velocity and v_0 is 1 a.u.), for an oxygen ion colliding with an aluminum target atom. Theoretical predictions are those of the plane-wave Born approximation, --- PWBA, the perturbed-stationary-state theory with Coulomb deflection and binding, — · — PSS(CB), and including polarization, ——— PSS(CBP). Total experimental K-hole production cross sections $\sigma_K(E)$ are obtained from our $\sigma_x(E)$ measurements using $\gamma_K(E) = 0.0426$. The dashed bar represents the shift in the value of $\sigma_K(E)$ as a result of using the fractional-parentage coefficient method of calculating $\gamma_K(E)$, as explained in the text. The inset shows Coulomb-excitation theory calculations: —— PSS(CBP) as in the main figure, and those including screening effects and electron capture as described in the text for O^{+8} (---), an equilibrium distribution of projectile charge states labeled O^{eq} (——), and for a neutral projectile O^{+0} (• • • •).

σ_K, even though multiple excitations in other shells may be taking place simultaneously.[40,41] The PWBA calculation drastically overestimates the cross section at energies below 10 MeV. The PSS(CB) theory falls below the data. The PSS(CBP) theory is in good agreement at energies above 10 MeV but is much too small at lower incident energies, in fact, by a factor 40 at 1 MeV.

The agreement between experiment and the PSS(CBP) theory may be fortuitous, since our projectiles are not point particles of nuclear charge Z_1 as assumed in the theory. Experimental results[19] indicate a variation of a factor 2–3 in the ionization cross section with the charge

state of the projectile for this projectile-target system. We attempt to reconcile these observations with Coulomb ionization theory by including in the total cross section the contribution due to capture of target K-shell electrons by the projectile, calculated according to Ref. 42, and by including screening effects of the projectile electrons in the cross section for ionization of target electrons to the continuum.

The magnitude of these contributions are shown in the inset of Fig. 8. The dashed curve is for an O^{+8} projectile, where electron capture dominates except at the highest energies. The magnitude of the electron-capture cross section is the difference between this curve and the PSS(CBP) curve. A Born approximation calculation[43] of the cross section for ionization to the continuum, which includes *ab initio* the effect of electron screening, indicates that the target cross section is decreased by ~10% for each K electron present on the projectile for the O-Al system; the presence of L electrons on the projectile does not significantly change the target cross section. This statement is valid in the 1–10 MeV/amu energy range for this projectile target system. We incorporate screening effects on the ionization cross section in the following manner. Coulomb and binding (C and B) effects are small impact parameter b dependent phenomena ($b \lesssim 1/Z_2$ a.u.). Moreover screening effects are important only at high velocities where Coulomb and binding effects are small. Therefore screening of the projectile is included via the calculation of Ref. 43. However, complete screening of the projectile by its K-shell electrons is assumed for the polarization (P) effect since this is a large ($b \simeq 2 - 3/Z_2$ a.u.) impact parameter phenomenon. The magnitude of the screening correction is the difference between the curve marked PSS(CBP), shown as the thick solid line, and that for neutral oxygen (O^{+0}), shown as the dotted line. Cross sections for O^{+q} ($q = 1-6$) which include electron capture and screening effects differ from that for O^{+0} by at most 10%. The thin solid line labeled O^{eq} is the ionization cross section when we include the above physical effects and assume an equilibrium distribution of charged states,[44] taken as that of the beam exiting the solid target. This curve represents our final Coulomb ionization cross sections, to which the data are compared. This curve is also shown in Fig. 9 as the light solid line.

We conclude that most of the aluminum K holes produced by oxygen bombardment of solid aluminum at projectile energies above 10 MeV are due to Coulomb ionization. Below 10 MeV some other mechanism must dominate the ionization process. We consider Pauli excitation, where exchange in

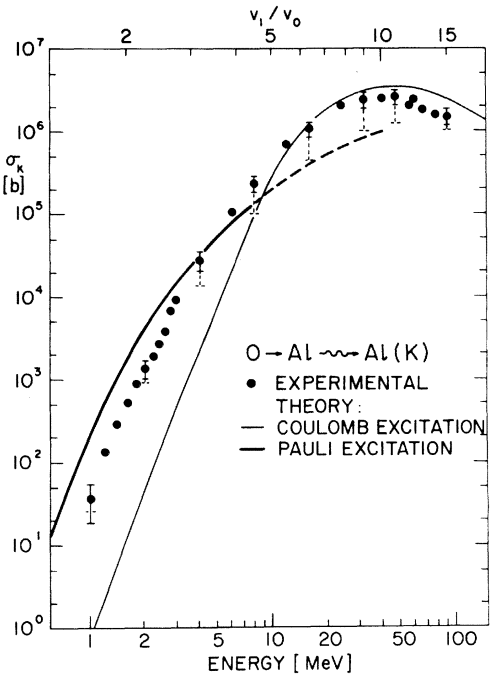

FIG. 9. Same as in Fig. 8 except that the theoretical curves are : —— O^{eq} Coulomb excitation as in the inset of Fig. 8, —— Pauli excitation using the statistical model as described in the text. The dashed section suggests the region where the model may be inapplicable.

the overlapping electron clouds of the colliding atoms is the dominating interaction. We apply the statistical model of Brandt and Jones,[45] based on a formulation of Mittleman and Wilets,[46] with scaling parameters $R_0 = 0.885(Z_1^{2/3} + Z_2^{2/3})^{1/2}$, and $\epsilon_{ion}^2/C = [(Z_1 + Z_2)/20]^3$ (in a.u.). This model gives the Pauli excitation cross sections for producing a K hole in both the incident and the target atom. We multiply these values with the branching ratio w of Meyerhof[47] to predict the Al(K) vacancy production cross section. The branching ratio is taken to be $w = (1 + e^x)^{-1}$, where $x = 27|I_2 - I_1| / [(I_1^{1/2} + I_2^{1/2})v_1]$ given in terms of I_1 and I_2, the K-shell binding energies[48] (in keV) of the projectile and target atom and of the incident projectile velocity v_1 in a.u. The semiempirical form of w given by Stolterfoht, Ziem, and Ridder[49] gives the same values (within 30%). The resulting Al(K) Pauli-excitation cross sections are displayed as the heavy solid curve in Fig. 9. We conclude that at oxygen energies below 10 MeV, corresponding to velocities $v_1 < Z_1^{2/3} v_0$, the dominant mechanism for creating K holes in aluminum with oxygen bombardment is Pauli excitation. When $v_1 > Z_1^{2/3} v_0$ the projectile is essentially stripped, and Coulomb ionization dominates. It is important

to note that our conclusions concerning the mechanisms of producing aluminum K-shell vacancies with oxygen bombardment do not depend on a specific choice of the fluorescence yield.

V. SUMMARY

We have determined the total Al(K) ionization cross sections for collisions of swift oxygen ions in solid aluminum targets. In order to do so, some large effects must be taken into consideration. Among these are the effects of the noncharacteristic radiation band, the recoil effect, and the change in fluorescence yield with the number and type of L holes simultaneously present with the K hole at the time of x-ray emission. The effects of the NCR band and that of recoils can be fully taken into account, but obtaining accurate values of the average fluorescence yield is still a difficulty. In addition, the possibly large charge-state dependence of the cross sections is unobtainable from our solid target data.

Comparison of our experimental results with theory shows that, for our conditions, K-shell holes in aluminum are produced primarily by Coulomb ionization at oxygen projectile velocities $v_1 > Z_1^{2/3} v_0$. For $v_1 < Z_1^{2/3} v_0$ the data is much higher than Coulomb ionization theory which includes binding, polarization, Coulomb deflection, screening, and electron-capture effects. Electron capture is important in this velocity range, but does not dominate the cross section for the solid targets we used. The large experimental cross sections at $v_1 < Z_1^{2/3} v_0$ we attribute to Pauli excitation, and a comparison of the data to a calculation using the statistical model of inner-shell vacancy production combined with vacancy transfer shows good agreement. This means that for oxygen incident on aluminum, where $Z_1/Z_2 = 0.62$, Pauli excitation is already important at projectile velocities less than about $Z_1^{2/3} v_0 = 4v_0$, and is the dominant mechanism of excitation to velocities of $1.6v_0$, which is the lowest velocity at which we could obtain measurable cross sections.

ACKNOWLEDGMENTS

We wish to acknowledge the many fruitful discussions with G. Basbas, W. Brandt, G. Lapicki, and A. Schwarzschild. We would like to thank the BNL Tandem operating staff and J. Riley of BNL for providing the required ion beams, and F. Chen, M. Mourino, C. Peterson, and A. Ratkowski for their assistance during the experiments.

---

*Work supported by the U. S. Energy Research and Development Administration.

[1]For a collection of work on this subject see *Proceedings of the International Conference on Inner-Shell Ionization Phenomena and Future Applications, 1972, Atlanta*, edited by R. W. Fink, S. T. Manson, J. M. Palms, and P. V. Rao (U.S. AEC, Oak Ridge, Tenn., 1973).

[2]F. W. Saris, W. F. van der Weg, H. Tawara, and R. Laubert, Phys. Rev. Lett. 28, 717 (1972).

[3]K. Taulbjerg and P. Sigmund, Phys. Rev. A 5, 1285 (1972).

[4]K. Taulbjerg, B. Fastrup, and E. Laegsgaard, Phys. Rev. A 8, 1814 (1973).

[5]F. P. Larkins, J. Phys. B 4, L29 (1971).

[6]C. P. Bhalla, Phys. Rev. A 12, 122 (1975).

[7]P. Richard, I. L. Morgan, T. Furuta, and D. Burch, Phys. Rev. Lett. 23, 1009 (1969).

[8]D. Burch and P. Richard, Phys. Rev. Lett. 25, 983 (1970).

[9]A. R. Knudson, D. J. Nagel, P. G. Burkhalter, and K. L. Dunning, Phys. Rev. Lett. 26, 1149 (1971).

[10]J. R. Macdonald, L. Winters, M. D. Brown, T. Chiao, and L. D. Ellsworth, Phys. Rev. Lett. 29, 1291 (1972).

[11]W. Brandt, R. Laubert, and I. Sellin, Phys. Rev. 151, 56 (1966).

[12]E. Merzbacher, and H. W. Lewis, *Encyclopedia of Physics*, edited by S. Flügge (Springer-Verlag, Berlin, 1958), Vol. 34, p. 166.

[13]D. I. Porat and K.Ramavataram, Proc. Phys. Soc. Lond. 77, 97 (1961).

[14]J. H. Ormrod, J. R. Macdonald, and H. E. Duckworth, Can. J. Phys. 43, 275 (1965).

[15]L. C. Northcliffe and R. F. Schilling, Nuclear Data Tables A7, 233 (1970).

[16]J. Lindhard, V. Nielsen, and M. Scharff, K. Dan. Vidensk. Selsk. Mat.-Fys. Medd. 36, No. 10 (1968).

[17]P. B. Needham, Jr. and B. D. Sartwell, Phys. Rev. A 2, 27 (1970).

[18]W. Brandt and R. Laubert, Phys. Rev. Lett. 24, 1037 (1970).

[19]W. Brandt, R. Laubert, M. Mourino, and A. Schwarzschild, Phys. Rev. Lett. 30, 358 (1973).

[20]G. Basbas, W. Brandt, and R. Laubert (to be published).

[21]The aluminum targets were supplied by Yissum Research Development Company, Jerusalem, Israel.

[22]ABACUS calculations of E. Auerbach of Brookhaven National Laboratory (private communication).

[23]R. Laubert, H. Haselton, J. R. Mowat, R. S. Peterson, and I. A. Sellin, Phys. Rev. A 11, 135 (1975).

[24]W. Brandt and R. Laubert, Phys. Rev. A 11, 1233 (1975).

[25]M. Sakisaka (1971). These results are obtained from Fig. 3.21 in Ref. 27. A value of $\gamma_K = 0.038$ was assumed to obtain σ_x. Reference 27 refers to these results as a private communication.

[26]D. Burch and P. Richard (1971). These results are obtained from Fig. 3.24 of Ref. 27. A value of $\gamma_K = 0.038$ was assumed to obtain σ_x. Reference 27 refers to these results as a private communication.

[27]J. D. Garcia, R. J. Fortner, and T. M. Kavanagh,

Rev. Mod. Phys. 45, 111 (1973).
[28]D. K. Olsen, C. F. Moore, and R. L. Kauffman, Phys. Lett. 44A, 109 (1973).
[29]F. Hopkins, D. O. Elliott, C. P. Bhalla, and P. Richard, Phys. Rev. A 8, 2952 (1973).
[30]R. L. Watson, F. E. Jenson, and T. Chiao, Phys. Rev. A 10, 1230 (1974).
[31]A. R. Knudson, D. J. Nagel, and P. G. Burkhalter, Phys. Lett. 42A, 69 (1972).
[32]P. Richard, R. L. Kauffman, J. H. McGuire, C. F. Moore, and D. K. Olsen, Phys. Rev. A 8, 1369 (1973).
[33]A. R. Knudson, P. G. Burkhalter, and D. J. Nagel, see Ref. 1, p. 1675.
[34]C. P. Bhalla, Phys. Lett. 46A, 185 (1973).
[35]F. J. McGuire, Phys. Rev. 185, 1 (1969).
[36]W. Bambynek, B. Crasemann, R. W. Fink, H.-U. Freund, H. Mark, C. D. Swift, R. E. Price, and P. V. Rao, Rev. Mod. Phys. 44, 715 (1972).
[37]G. S. Khandelwhal, B. H. Choi, and E. Merzbacher, At. Data 1, 103 (1969).
[38]G. Basbas, W. Brandt, and R. H. Ritchie, Phys. Rev. A 7, 1971 (1973).
[39]G. Basbas, W. Brandt, and R. Laubert, Phys. Rev. A 7, 983 (1973).
[40]J. H. McGuire and J. R. Macdonald, Phys. Rev. A 11, 146 (1975).
[41]G. Basbas, Bull. Am. Phys. Soc. 20, 675 (1975).
[42]W. Losonsky and G. Lapicki, Bull. Am. Phys. Soc. 20, 638 (1975); G. Lapicki, and W. Losonsky, Bull. Am. Phys. Soc. 21, 32 (1976).
[43]G. Basbas, in *Electronic and Atomic Collisions, Abstracts of Papers on the Ninth International Conference on the Physics of Electronic and Atomic Collisions, Seattle, Washington, 1975*, edited by J. S. Risley, and R. Geballe (Univ. of Washington Press, Seattle, 1975), p. 502.
[44]J. B. Marion and F. C. Young, *Nuclear Reaction Analysis* (North-Holland, Amsterdam, 1968), p. 43.
[45]W. Brandt and K. W. Jones, Phys. Lett. 57A, 35 (1976).
[46]M. H. Mittleman and L. Wilets, Phys. Rev. 154, 12 (1967).
[47]W. E. Meyerhof, Phys. Rev. Lett. 31, 1341 (1973).
[48]J. A. Bearden, Rev. Mod. Phys. 39, 78 (1967).
[49]N. Stolterfoht, P. Ziem, and D. Ridder, J. Phys. B 7, L404 (1974).